Multiple-histogram Monte Carlo study of the Ising antiferromagnet on a stacked triangular lattice

Alex Bunker, B. D. Gaulin, and C. Kallin
Department of Physics and Astronomy, McMaster University, Hamilton, Ontario, L8S 4M1, Canada
(Received 21 January 1993; revised manuscript received 16 August 1993)

The nearest neighbor Ising antiferromagnet on a stacked triangular lattice is a frustrated cooperative system in which it is known that at least two long-range ordered states exist at low temperature. This model has also been of considerable interest as it is known to be a reasonable description of two antiferromagnetic insulators, $CsCoBr_3$ and $CsCoCl_3$. It has also been the subject of previous theoretical and simulation studies which have yielded conflicting results for the critical phenomena displayed near the transition from the paramagnetic to the high-temperature ordered phase. We have carried out a detailed Monte Carlo study of this system using the recently developed multiple-histogram technique and finite-size scaling analysis, with the purpose of extracting estimates for the critical exponents relevant to this continuous transition. Our results give $\beta = 0.311(4)$, $\gamma = 1.43(3)$, $\alpha = -0.05(3)$, and $\nu = 0.685(3)$ which are not in agreement with previous Monte Carlo work. In addition, although they are close to the expectations from previous symmetry arguments, there are systematic differences between our results and these theoretical predictions. A possible interpretation of these Monte Carlo exponent estimates is that they do not correspond to those calculated for any known universality class, and add to the growing number of simple models of interacting spins, in which geometrical frustration is relevant, which appear to exhibit novel critical behavior. Finally, we have examined the evolution of real-space spin configurations and have seen that a buildup of correlations between anti-phase-domain walls, or solitons, along the stacking direction precedes the transition, an observation which is consistent with recent neutron-scattering measurements on $CsCoBr_3$.

I. INTRODUCTION

A spin system is said to be frustrated if the pairwise interactions between spins cannot all be simultaneously satisfied. Such systems often display interesting statistical mechanical behavior because of the complex orderings that can arise when the spins arrange themselves in an energetic compromise. Frustration requires competing interactions, and can be due to randomness, as in a spin glass, or can arise from the geometry of the lattice.

The Ising model with nearest-neighbor, antiferromagnetic interactions on a triangular lattice is perhaps the best known example of a geometrically frustrated spin system. Wannier[1] showed in the 1950s that this system is disordered at all finite temperatures, and has a critical point at $T = 0$. Lattices which locally frustrate nearest-neighbor antiferromagnetic interactions are based on two geometrical units. These are triangles and tetrahedra which form the basis for triangular, Kagomé,[2] pyrochlore,[3] and face-centered-cubic structures. Considerable recent interest has been generated in this area by experimental studies on magnetic materials which are well described by antiferromagnetically coupled spins on these types of lattices.

In the stacked triangular lattice (STL), also known as the hexagonal lattice, the triangular planes, which frustrate antiferromagnetic interactions within them, are simply stacked directly over each other. Therefore the interactions along the stacking direction are nonfrustrated regardless of whether these interactions are ferromagnetic or antiferromagnetic. The nonfrustrated coupling along the stacking direction allows the STL antiferromagnet to undergo a finite temperature phase transition. For the case of both XY and Heisenberg spins with nearest-neighbor antiferromagnetic interactions on the STL, Kawamura[4] has performed extensive analyses of the critical behavior, by conventional Monte Carlo as well as by analytical methods. He argued that both models display novel critical behavior and belong to new universality classes, a prediction which has recently gained considerable experimental support.[5] Some controvery has been added to this field, at least for Heisenberg spins, by recent field theory in $2 + \epsilon$ dimensions which contends that the behavior either should be weakly discontinous, $O(n = 4)$, or should display tricritical mean field behavior.[6]

Recently, neutron diffraction from FeF_3, which is a cubic pyrochlore antiferromagnet, showed the sublattice magnetization exponent β to be anomalously low, $\beta = 0.18 \pm 0.02$.[7] The authors of this study also carried out a histogram Monte Carlo analysis with finite-sized scaling on classical Heisenberg spins, coupled with antiferromagnetic nearest-neighbor interactions and ferromagnetic third-nearest-neighbor interactions on the pyrochlore lattice. This is believed to be an appropriate model for FeF_3. These results indicate that, for this model also, the transition from the paramagnetic to the long-range ordered state is characterized by critical exponents which do not correspond to any known universality class. This model with antiferromagnetic, nearest-

neighbor-only interactions has also been studied[8] by histogram Monte Carlo analysis, and these results are consistent with the absence of long-range order at any finite temperature. This is also the conclusion reached from conventional Monte Carlo analysis of classical antiferromagnetically coupled Ising spins on the pyrochlore lattice.[9]

The classical, antiferromagnetic Ising model on the STL has been studied in some detail recently.[10–14] It is known that it displays two ordered states at low temperatures. The high-temperature ordered state corresponds to a $(1,-1,0)$ magnetic sublattice structure in which the magnetic unit cell consists of a triad of three nearest-neighbor spins. Spins on two of the sublattices form an up-down pair, while the third is randomly oriented. At lower temperatures the system enters another ordered state characterized by the $(-1,\frac{1}{2},\frac{1}{2})$ sublattice structure. The emphasis in this paper is to investigate the critical phenomena near the transition at T_N from the paramagnetic to high-temperature ordered state with the $(1,-1,0)$ sublattice structure.

At present there are conflicting theoretical results for the critical behavior at T_N of this model. The results of a symmetry argument[10] indicate that the transition should belong to the three-dimensional (3D) XY universality class with critical exponents $\beta = 0.346(9)$, $\gamma = 1.316(9)$, $\nu = 0.669(7)$, and $\alpha = -0.007(9)$.[15] However, previous conventional Monte Carlo simulation work (without a comprehensive finite-size scaling analysis) has indicated that critical exponents close to those of a mean field tricritical point, $\beta = 0.19(10)$, $\gamma = 1.15(5)$, $\alpha = 0.5(1)$, and $\nu = 0.47$, are relevant for this transition.[12] Netz and Berker[13] have argued that this discrepancy is due to the proximity of the transition to a tricritical region at finite field which influences the critical behavior except in a very narrow region around T_N. In this paper we will present results of a multiple-histogram Monte Carlo study, together with a finite-size scaling analysis which predicts critical exponents that differ significantly from mean field tricritical point exponents and, to a lesser extent, from those of the 3D XY model. These exponents are extracted from a finite-size scaling analysis of the behavior right at the transition T_N and, hence, would only be influenced by the existence of a tricritical region to the extent that T_N varies from one lattice size to another.

There are two possible explanations for the discrepancy between our Monte Carlo exponent estimates and those predicted by the 3D XY model.[15] Systematic errors may exist in either our calculations and analysis, which would have to be substantialy greater than the statistical errors, or in the predictions for the 3D XY model.[15] Alternatively, this Ising model may belong to a new universality class, as has already been suggested for the XY and Heisenberg antiferromagnets on this lattice.[4] However, it is important to note that earlier work[4,7] suggesting new universality classes for frustrated systems applies only to vector spin systems where there can be chiral order and, hence, does not apply to the Ising on the STL. Thus, if systematic errors could in fact be ruled out, a completely new explanation for the existence of a new universality class (possibly involving the role of frustration induced disorder) would be needed.

In zero external magnetic field, the case we are interested in, symmetry principles dictate that the physics of the system will be identical if the interactions between classical spins on adjacent triangular layers are ferromagnetic or antiferromagnetic. Since the analysis is simpler for the ferromagnetic case, this is the model we will use. The Hamiltonian is then

$$H = J_0 \sum_{\langle i,i'\rangle,j} \sigma_{i,j}\sigma_{i',j} - J_1 \sum_{i,j} \sigma_{i,j}\sigma_{i,j+1}, \tag{1}$$

where $\sigma_{i,j} = \pm 1$ denotes the spin at site i,j, and J_0 is positive and accounts for the the nearest-neighbor, antiferromagnetic exchange in the triangular lattice plane (the ab plane); J_1 is also positive, and produces the nearest-neighbor, ferromagnetic spin coupling along the stacking axis (the c axis). Therefore, $\langle i,i'\rangle$ runs over the nearest-neighbor pairs in the ab plane, and j is the index along the c axis.

This model Hamiltonian is reasonably close to that which describes the antiferromagnetic insulators $CsCoBr_3$ and $CsCoCl_3$.[16] The interactions between the spin $\frac{1}{2}$ magnetic moments localized at the Co^{2+} site are antiferromagnetic both along c and in the ab plane. These isostructural, hexagonal materials are quasi-one-dimensional magnets with a ratio of the strength of exchange interaction along c to that within the ab plane of $\sim$ 160:1. In addition, the moments are not completely Ising-like and a small amount of transverse spin coupling appears in the Hamiltonian. Although there are some potentially important differences between the real materials and the model system studied here, we expect the analysis of this simple model to be of some importance in elucidating their critical phenomena. In most of the work described below, we have chosen $J_0 = J_1$, since the ratio J_1/J_0 is irrelevant to the asymptotic critical behavior and the isotropic case is technically easier for Monte Carlo methods.

The status of the experimental field is presently unclear. Three determinations of the β exponent, which describes the rise of the sublattice magnetization from zero at the phase transition, have been made on the Co-based magnetic insulators. Mekata and Adachi[17] obtained a value of $\beta = 0.35 \pm 0.02$ for $CsCoCl_3$, a value which is consistent with predictions of the 3D XY model. Yelon *et al.*[18] obtained a value of 0.31 ± 0.02, while Farkas *et al.*[19] obtained the value 0.22 ± 0.02 for $CsCoBr_3$. The β value determined by Yelon *et al.* is consistent with the 3D Ising model, while that of Farkas *et al.* is close to that expected from tricritical mean field theory ($\beta = 0.25$). Very recently, Wang *et al.*[20] have performed critical heat capacity measurements on the same sample of $CsCoBr_3$ studied by Farkas *et al.*,[19] and obtained values of $\alpha = -0.027(5)$ and $A_+/A_- = 1.13(7)$, where α describes the cusp in the heat capacity at T_N while A_+/A_- is the critical ratio of heat capacity amplitudes. While these values are not far from those expected theoretically from the 3D XY model, the discrepancy is potentially interesting in light of the direction of the difference between the measured α and that predicted theoretically (the measured value is more negative), and the conclu-

sions which we will present in this paper. It is worth noting, however, that these measurements on $CsCoBr_3$ are in remarkable agreement with those on the superfluid transition in liquid ^4He,[21] another system which is expected to belong to the 3D XY universality class. Clearly, a comprehensive experimental program of measuring the critical properties of these materials is required.

The remainder of this paper is organized as follows. In Sec. II, there is a description of our Monte Carlo method, including the multiple-histogram method, finite-size scaling, and an algorithm to estimate the critical exponents. The Monte Carlo results are described in Sec. III, followed by a discussion of their significance in Sec. IV.

II. USE OF THE MONTE CARLO METHOD TO STUDY CRITICAL PHENOMENA

A. The histogram Monte Carlo method

Most Monte Carlo simulation work utilizes the Metropolis algorithm in order to generate new spin configurations at a particular temperature. One then goes on to calculate thermodynamic averages of observables. In a surprisingly recent development, Ferrenberg and Swendson[22] realized that this method did not make full use of all of the data held in the actual distribution of the sampled state. They developed the single-histogram Monte Carlo method to take advantage of this additional information.

A difficulty with the single-histogram method arises due to the fact that at any temperature the probability distribution in energy is rather narrow. This was improved by the development of the multiple-histogram Monte Carlo method, also by Ferrenberg and Swendson,[23] in which data taken at different temperatures is combined so as to produce a more accurate determination of the relevant distribution. This multiple-histogram method permits the determination of accurate estimates of observables over a relatively wide range of temperature.

B. The measurement of T_N

An accurate estimate of T_N is an essential first step to the study of critical phenomena. There are several observables that have extrema at T_N. These are

$$\langle \chi \rangle = \frac{N}{(k_B T)} (\langle O^2 \rangle - \langle O \rangle^2), \tag{2}$$

$$\langle C_H \rangle = \frac{1}{N k_B T^2} (\langle E^2 \rangle - \langle E \rangle^2), \tag{3}$$

$$\langle O' \rangle = \frac{\partial O}{\partial \frac{1}{k_B T}} = \langle OE \rangle - \langle O \rangle \langle E \rangle, \tag{4}$$

$$\langle (O^2)' \rangle = \frac{\partial O^2}{\partial \frac{1}{k_B T}} = \langle O^2 E \rangle - \langle O^2 \rangle \langle E \rangle, \tag{5}$$

$$\langle (\ln O)' \rangle = \frac{\partial \ln O}{\partial \frac{1}{k_B T}} = \frac{\langle OE \rangle}{\langle O \rangle} - \langle E \rangle, \tag{6}$$

$$\langle (\ln O^2)' \rangle = \frac{\partial \ln O^2}{\partial \frac{1}{k_B T}} = \frac{\langle O^2 E \rangle}{\langle O^2 \rangle} - \langle E \rangle, \tag{7}$$

$$\langle V_L \rangle = 1 - \frac{\langle E^4 \rangle}{3 \langle E^2 \rangle^2}, \tag{8}$$

$$\langle U_L' \rangle = \frac{\partial U_L}{\partial \frac{1}{k_B T}} = \langle U_L E \rangle - \langle U_L \rangle \langle E \rangle, \tag{9}$$

$$\langle U_L \rangle = 1 - \frac{\langle O^4 \rangle}{3 \langle O^2 \rangle^2}, \tag{10}$$

where O is the order parameter, $\langle U_L \rangle$ is the fourth order cumulant, and $\langle V_L \rangle$ is the fourth order energy cumulant.

A Monte Carlo approximation of all these observables can be obtained if, for each state sampled, the values of E, O, O^2, and O^4 are calculated. Since the only external parameter being considered is T, it is necessary to store only the energy values in a histogram. Each O, O^2, and O^4 value recorded at a given energy E is then simply summed into an average. In this way values for $\langle O(E) \rangle$, $\langle O(E)^2 \rangle$, and $\langle O(E)^4 \rangle$ are obtained.

C. Other information in P_M

The value of an observable $\langle A \rangle$ is only part of the information about the cooperative phenomena of a given system that can be obtained from a Monte Carlo simulation. Further information is contained in the structure of the probability distribution of states at T_N, $P(T_N, E)$. If a double-peaked structure is observed, one may be able to extract information about the order of the transition.[24] Note that a double-peak structure does not necessarily imply that the the transition is first order (or discontinuous).[25] One can also examine the real-space, spin configurations with the Monte Carlo simulation. This is useful in elucidating changes in spin topology in the vicinity of the phase transition, and can shed light on the physical mechanism which drives a particular phase transition. Neutron-scattering experiments probe the spin correlations in reciprocal space, and this real-space information information on model systems can be a useful complement to the results of such experiments on real materials.

D. Finite-size scaling

The finite size scaling laws, as derived by Fisher[26] and Landau,[27] for a continuous, or second order, transition are given by

$$F(t, L) = L^{(2-\alpha)/\nu} \mathcal{F}^0(x), \tag{11}$$

$$O(t, L) = L^{-\beta/\nu} \mathcal{X}^0(x), \tag{12}$$

$$\chi(t,L) = L^{\gamma/\nu}\mathcal{Y}^0(x), \tag{13}$$

$$C_H(t,L) = C_0 + L^{\alpha/\nu}\mathcal{Z}^0(x), \tag{14}$$

where $x = tL^{1/\nu}$, $t = \frac{|T-T_N|}{T_N}$, and T_N is the transition temperature for lattice size L. At the phase transition, $t = 0$, we have the special case of Eqs. (12)–(14):

$$C_{H\max}(L) = C_0 + C_1 L^{\alpha/\nu}, \tag{15}$$

$$\chi_{\max}(L) \propto L^{\gamma/\nu}, \tag{16}$$

$$O_{T_N(\infty)}(L) \propto L^{-\beta/\nu}. \tag{17}$$

Other scaling relations relevant to a continuous transition are

$$U'_{L\max}, (\ln O)'_{\max}, (\ln O^2)'_{\max} \propto L^{1/\nu}. \tag{18}$$

Each of these observables has a separate $T_N(L)$. For large L the $T_N(L)$ scale as

$$T_N(L) = T_N(\infty) + C_A L^{-1/\nu}. \tag{19}$$

It is possible to apply this analysis to relatively small lattices; however, a new correction term $L^{-\theta/\nu}$ must be included in order to take into account the effect of irrelevant scaling fields and nonlinearities in the scaling variable. Including this term, we have

$$T_N(L) = T_N(\infty) + C_A L^{-1/\nu} + D_A L^{-\theta/\nu}. \tag{20}$$

T_N for each observable has a separate and independent C_A and D_A, but a common θ.

For a discontinuous, or first order, transition the following finite-size scaling laws apply:

$$C_{H\max} = C_1 + C_2 L^d, \tag{21}$$

$$\chi_{\max} = \chi_1 L^d, \tag{22}$$

$$T_N(L) = T_N(\infty) + C_A L^{-1/d}. \tag{23}$$

E. An algorithm for determining critical exponents

Below we outline the procedure which we used to study the critical phenomena of the model in question using the multiple-histogram Monte Carlo method.

(1) Roughly determine the critical region $T_N \pm \delta T_N$, and create R histograms spanning the T range of the phase transition, storing the values of the histogram $H(T_i,E,L)$, as well as $O(T_i,E,L)$, $O^2(T_i,E,L)$, $O^4(T_i,E,L)$ for several values of finite size L.

(2) Calculate f for each of the R histograms at each lattice size L. Find the values of $\langle E_M\rangle$, $\langle E_M^2\rangle$ $\langle E_M^4\rangle$, $\langle O_M\rangle$, $\langle O_M^2\rangle$, $\langle O_M^4\rangle$ over a range of T spanning the critical region, and use these values to calculate all the observables given in Eqs. (2)–(10).

(3) Determine the order of the phase transition. If the distribution $P_M(E)$ at T_N is double peaked, the method of Lee and Kosterlitz[24] may be applied. If not, extrapolate the fourth order energy cumulant $\langle V_L\rangle_{\min}$ to $L = \infty$ to see if it approaches a constant $V^* = 2/3$ (indicating a continuous transition) or $V^* < 2/3$ (indicating a first order transition). If the transition is continuous, then the critical exponents can be determined from the following steps.

(4) Determine ν from the finite-size scaling of the maxima of U'_L, $(\ln O)'$, $(\ln O^2)'$ [Eq. (18)]. This is done by graphing $\ln L$ vs ln(maxima). Similarly determine γ by graphing $\ln L$ vs $\ln\chi_{\max}$.

(5) Determine all the $T_N(L)$ given by the observables of Eqs. (10)–(18) and plot these vs $L' = L^{-1/\nu}$. $T_N(\infty)$ can be determined by fitting to the form $B + C_{A_i}L' + D_{A_i}L'^{\theta}$ and $T_N(L=\infty) = \overline{B}$, where $\overline{B}$ is the average of B over all the observables.

(6) With the results for ν and $T_N(\infty)$, determine β from a graph of $\ln L$ vs $\ln O_{T_N}$. One can then use the scaling laws for $T \neq T_N$ to verify the results for β and γ. This is done by graphing $\ln(\chi L^{-\gamma/\nu})$ and $\ln(OL^{\beta/\nu})$ against $\ln(tL^{1/\nu})$, where $t = \frac{|T-T_N|}{T_N}$. If the critical exponents are chosen correctly, the results for each of these two graphs for different L should all fall onto the same line.

(7) Finally, approximate α using the scaling laws

$$2\beta + \alpha + \gamma = 2, \tag{24}$$

$$d\nu + \alpha = 2, \tag{25}$$

and verify this approximation by fitting Eq. (15) using the α from the scaling relations.

III. THE MONTE CARLO RESULTS

A. Check for anisotropic correlation lengths

The transition from the paramagnetic state to the high-temperature ordered state at T_N in the nearest-neighbor, Ising antiferromagnet on a STL was studied using the multiple-histogram Monte Carlo method described above. We first examined whether there was a significant anisotropy in the spin correlation length, that is, a difference between ξ_c and ξ_{ab}, for the Hamiltonian with isotropic exchange interactions J_0=J_1, since any significant anisotropy would require that the simulations be carried out on finite lattices which reflect this anisotropy. The correlation length in the c axis and ab plane was determined from a set of equilibrium states developed through the Monte Carlo method. The spin pair correlation function $C(r) = \langle S_i S_{i+r}\rangle$ can be determined individually for the two symmetry directions by restricting r to be either along the c axis or an axis in the ab plane. Assuming $C(r,T)$ is described by the Orstein-Zernike form, appropriate for a three-dimensional lattice, we have

$$C(r,T) = \frac{A}{r}e^{-r/\xi}. \tag{26}$$

Values for ξ were determined by graphing $\ln[rC(r,T)]$ vs r and $\xi(T) = -1/\text{slope}$. This expression for $C(r,T)$ is only valid for $r \gg$ the unit cell size. Because of finite-

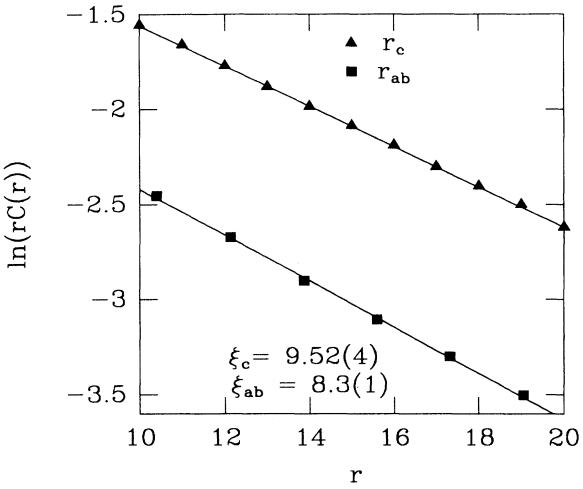

FIG. 1. The correlation length is determined from the slope of the $\ln[rC(r)]$ vs r plot, as described in the text. These results show that for isotropic interactions $J_0{=}J_1{=}1$, the anisotropy in the correlation lengths along c to that in the ab plane is small, $\sim 15\%$.

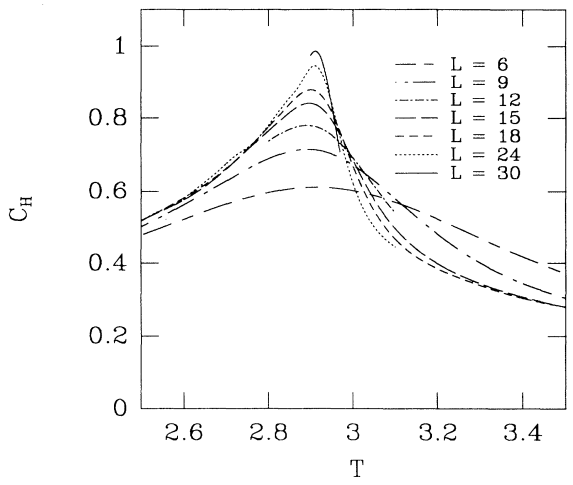

FIG. 2. The specific heat C_H is shown as a function of temperature near the phase transition temperature T_N for various lattice sizes $L \times L \times L$.

size effects, the result for $C(r,T)$ will also only be valid for $r \ll$ the lattice size. The valid region of $C(r,T)$ was taken to be the region for which the plot of $\ln[rC(r)]$ vs r was linear.

The procedure for determining the correlation lengths was to use 10^4 initialization steps and 3×10^3 sampled states at $T = 2.94$, in units of $J_0{=}J_1$, where T_N was known to be ~ 2.9. A lattice with dimensions $6 \times 6 \times 726$ was used to determine the c axis correlation length $C(r_c,T)$, while a lattice with dimensions $66{\times}66{\times}6$ was used to determine the ab plane correlation length $C(r_{ab},T)$. Thus the same number of spins were used in each ξ determination.

It was found that Eq. (34) provided a good description for $C(r,T)$ over the region $r = 10 \rightarrow 20$, for the determination of ξ in both directions. The graph in Fig. 1 shows this region, and the correlation lengths are found to be $\xi_c = 9.52(4)$ and $\xi_{ab} = 8.3(1)$. While we see an anisotropy in the c axis direction, it is small enough, $\xi_c/\xi_{ab} \approx 1.15$, that we can neglect it in our analysis of the critical phenomena.

The analysis of the critical phenomena at T_N was performed using simulations of the isotropic model, $J_0{=}J_1{=}1.0$. Analysis of the real-space spin and soliton correlations made use of simulations of both the isotropic model and a weakly one-dimensional model with $J_1{=}3.0$ and $J_0{=}1.0$.

B. The order parameter

The ordered state of the antiferromagnetic Ising model has a sixfold degeneracy. As the initial state used in the Monte Carlo routine is random, each of the six possible ordered domains will be equally accessible. The algorithm to determine the order parameter must determine the local order parameter of each of the possible domains and take the maximum. If M_i is the magnetization of sublattice i ($i = 1,2,3$), then the order parameter may be written as

$$O_{\text{Ising}} = [\max(M_1,M_2,M_3) - \min(M_1,M_2,M_3)]/2. \tag{27}$$

This is the form of the order parameter that we will use to calculate the various observables given in Eqs. (2)–(10).

C. The observables $\langle A \rangle_L$

The multiple-histogram method was used to determine the relevant observables as a continuous function of temperature T in the range of the phase transitions for lattice sizes $L = 6$, 9, 12, 15, 18, 24, and 30. Previous investigation of this model has shown $T_N \approx 2.9$ (in

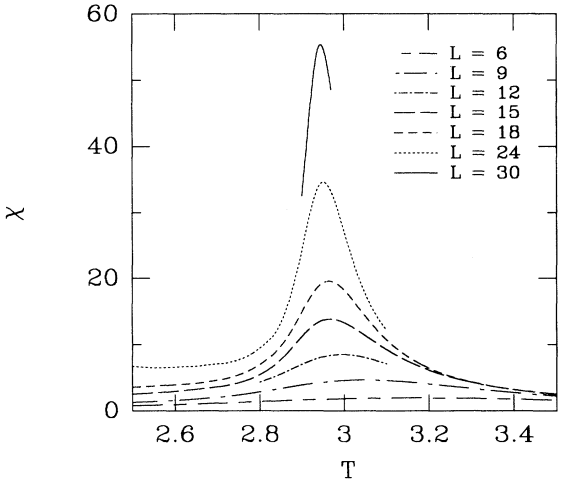

FIG. 3. The susceptibility χ is shown as a function of temperature near T_N, for various lattices sizes L.

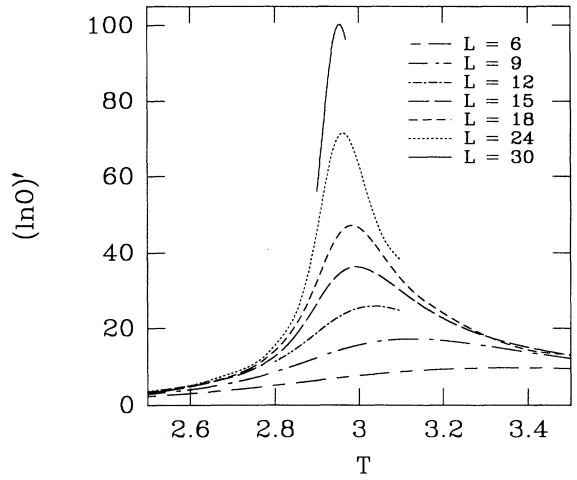

FIG. 4. The derivative of $\ln O$ with respect to the inverse temperature is shown as a function of temperature near T_N, for various lattice sizes L. O is the order parameter discussed in the text. A finite-size scaling analysis of these plots are used to determine the critical exponent ν.

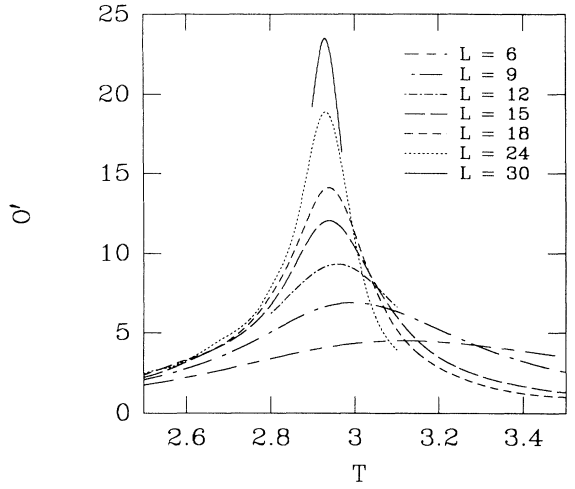

FIG. 6. The derivative of the order parameter O with respect to inverse temperature is shown as a function of temperature near T_N, for various lattice sizes L.

units of J_0=J_1=1.0). Histograms were produced around this temperature. For $L = 6$, histograms were made at $T = 2.6 \rightarrow 3.5$, in steps of 0.1, with 10^5 sampled states at each temperature, and at $T = 2.5$ with 5×10^4 sampled states. For $L = 9$ and 15, histograms were made at $T = 2.5 \rightarrow 3.5$, in steps of 0.1, with 10^5 sampled states at each temperature. For $L = 12$, histograms were made at $T = 2.8$, 2.9, 3.0, and 3.1 with 10^5 sampled states. For $L = 18$, histograms were made at $T = 2.5$, 2.6, 2.7, 2.8, 2.85, 2.95, 3.0, 3.1, 3.2, 3.3, 3.4, and 3.5 with 10^5 sampled states and at $T = 2.9$ with 2×10^5 sampled states. For $L = 24$, histograms were made at $T = 2.5$, 2.6, 2.7, 2.8, 2.9, 2.92, 3.0, and 3.1 with 10^5 sampled states. For $L = 30$, histograms were made at $T = 2.91$ and 2.935 with 10^5 sampled states and at $T = 2.97$ with 2×10^4 sampled states.

The data for these histograms were combined to determine the expectation values $\langle C_H \rangle$, $\langle \chi \rangle$, $|\langle O' \rangle|$, $|\langle (O^2)' \rangle|$, $|\langle (\ln O)' \rangle|$, $|\langle (\ln O^2)' \rangle|$, and $\langle V_L \rangle$ as a continuous function of temperature for the different lattice sizes. These results are shown in Figs. 2–8.

D. Critical phenomena

The data for $\langle A \rangle_L$ can now be used to estimate values of the critical exponents for this model. However, we must first convince ourselves that the transition is indeed continuous. First, the equilibrium probability distributions at T_N do not show a double-peak structure (see Fig. 9) and hence the method of Lee and Kosterlitz[24] is

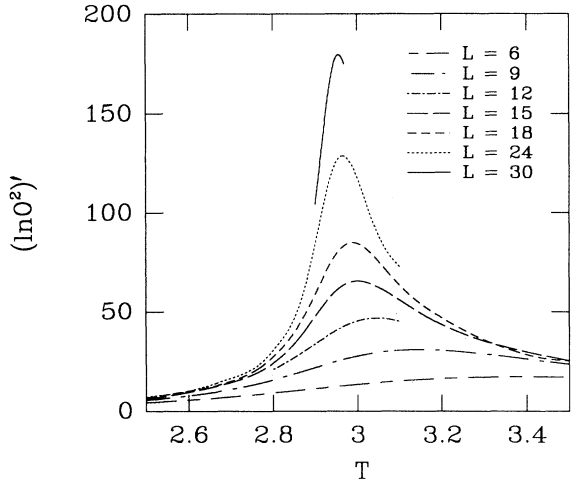

FIG. 5. The derivative with respect to the inverse temperature of $\ln(O^2)$, where O is the order parameter, is shown as a function of temperature near T_N, for various lattice sizes L.

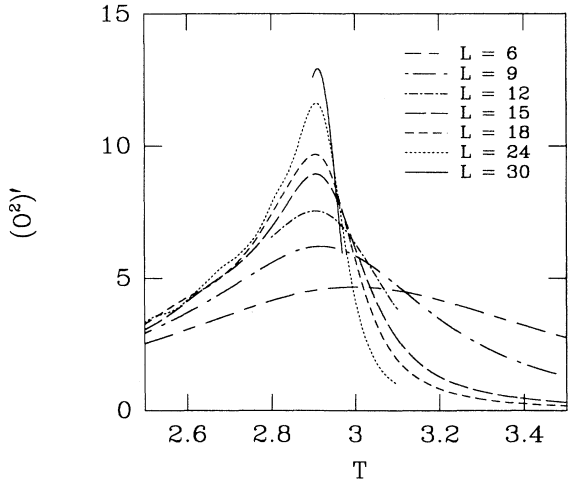

FIG. 7. The derivative with respect to inverse temperature of O^2, where O is the order parameter, is shown as a function of temperature near T_N for various lattice sizes L.

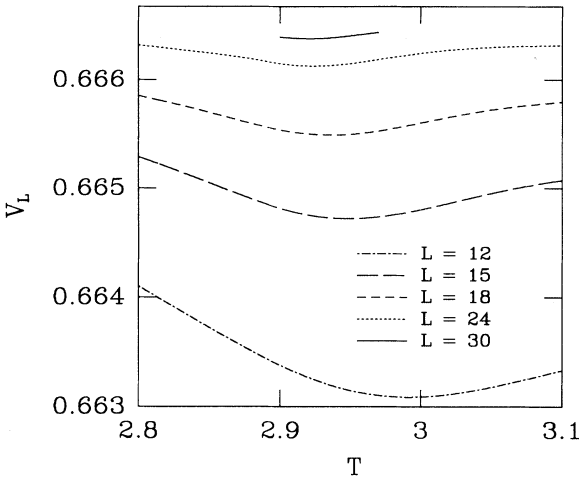

FIG. 8. The fourth order energy cumulant V_L is shown as a function of temperature near T_N, for the larger lattice sizes L.

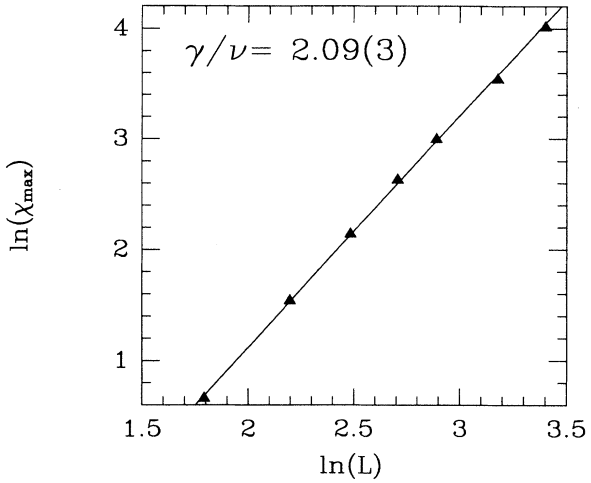

FIG. 10. The ratio of exponents, γ/ν, is determined from the slope of the $\ln(\chi_{\max})$ vs $\ln L$ plot, and found to be γ/ν=2.09(3). Here $\chi_{\max}$ is the maximum susceptibility as a function of temperature, for fixed L, as shown in Fig. 3. These results show that the transition is second order since $\gamma/\nu < 3$.

inapplicable to our problem. Second, we can study how the suceptibility maximum $\chi_{\max}$, scales with lattice size L. As discussed above, χ scales as L^d for a discontinuous transition and as $L^{\gamma/\nu}$ for a continuous one. Thus if the slope of the plot of $\ln\chi_{\max}$ vs $\ln L < 3$, then we know the transition is second order. As shown in Fig. 10 the slope of this graph from our simulations was found to be = 2.09(3), indicating that the transition is indeed continuous with the ratio $\gamma/\nu = 2.09$. Finally, the most reliable method is to determine the asymptotic value of the fourth order energy cumulant V^* and see if it is less than or equal to 2/3. This is plotted in Fig. 11, which clearly shows V^* to be approaching 2/3 for large L. We estimate that $V^*(L = \infty) = 0.6667(1)$.

Now that the transition has been determined to be continuous, and therefore that critical exponents are meaningful, we will determine ν in order to find γ and $T_N(L = \infty)$. As already mentioned, ν is found from plot-

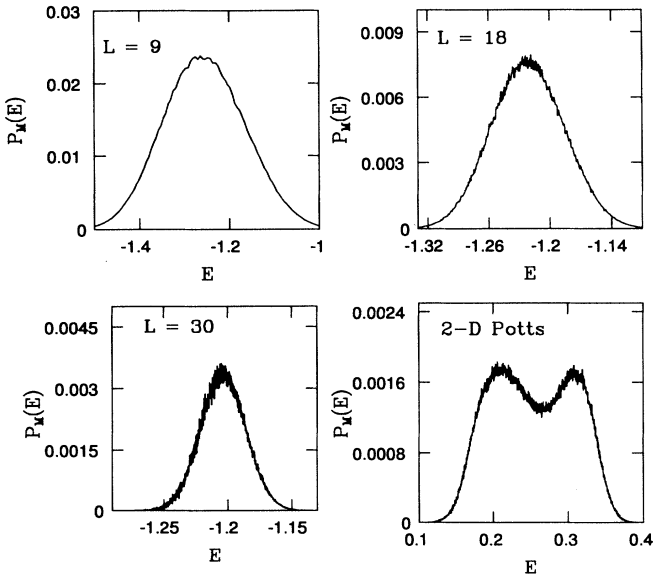

FIG. 9. The equilibrium probability distribution $P_M(E)$ at T_N is shown for lattice sizes L = 9, 18, and 30. The critical temperature T_N is determined from the specific heat. Note the single-peak distribution indicating the second order nature of the transition. For comparison, the probability distribution of the three-state antiferromagnetic Potts model on a triangular lattice at T_N = 0.63 is also shown. This model is known to display a discontinuous phase transition.

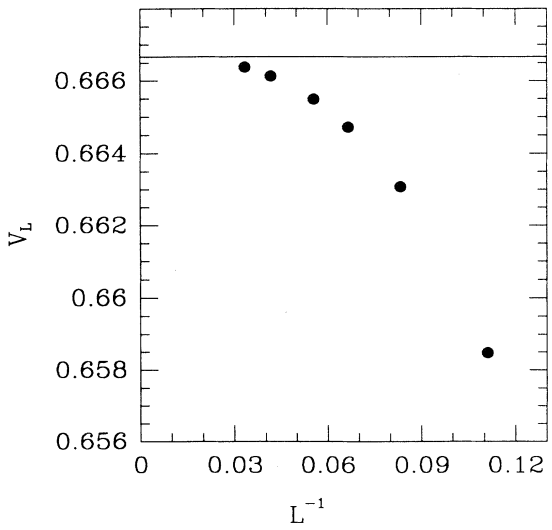

FIG. 11. The fourth order energy cumulant is shown as a function of system size L. These results extrapolate to V^* = 0.6667(1) for $L \to \infty$, as expected for a continuous phase transition. The solid horizontal line denotes $V_L = 2/3$.

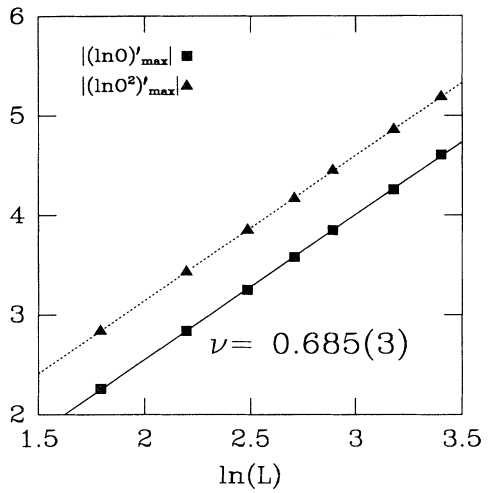

FIG. 12. The critical exponent ν is determined from the slope of the $|(\ln O)'_{\max}|$ and $|(\ln O^2)'_{\max}|$ vs $\ln L$ plots, as described by Eq. (26). Here, O is the order parameter, the primes denote derivatives with respect to inverse temperature, and the maxima are determined from the peaks in Figs. 4 and 5, for each L. The resulting exponent is ν=0.685(3).

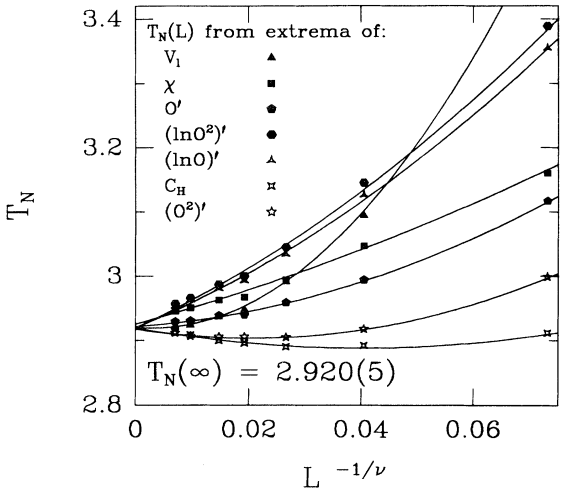

FIG. 13. The transition temperatures, as listed in Table I, are plotted as a function of $L^{-1/\nu}$, where $\nu = 0.685$. The solid curves show the best fit to Eq. (28), which was found for $\theta = 2$. The resulting $T_N(L \to \infty) = 2.920(5)$.

ting $\ln[(\ln O)'_{\max}]$ and $\ln[(\ln O^2)'_{\max}]$ vs $\ln L$. One can also use $(U_L)'_{\max}$ but this was not measured since the critical properties of this observable have a very large L dependence which makes the finite-size scaling analysis of it unreliable. This analysis results in an estimate of $\nu = 0.685(3)$ which is taken from the graph shown in Fig. 12. As we had previously determined the ratio of γ to ν to be 2.09, this also determines an estimate for $\gamma = 1.43(3)$.

Using this value of ν, $T_N(L = \infty)$ can be found from Eq. (28). In order to do this we must find a value of θ that will best fit all the $T_N(L)$. The T_N for $L = 6$, 9, 12, 15, 18, 24, and 30, for all the measured observables, are listed in Table I. These values for T_N are plotted against $L^{-1/\nu}$ in Fig. 13, and the best fit to Eq. (28) was found for $\theta = 2$. This results in $T_N(L = \infty) = 2.920(5)$.

With a good determination of T_N, β can be found via $O(L)_{T_N} \propto L^{-\beta/\nu}$. $\ln O_{T_N(L=\infty)}$ is plotted against $\ln L$ in Fig. 14, and this results in our estimate for $\beta = 0.311(4)$. As we now have estimates of three critical exponents, we can use both scaling and hyperscaling relations to determine our estimate for the fourth, α. With $\nu = 0.685(3)$, $\gamma = 1.43(3)$, and $\beta = 0.311(4)$ both scaling laws, $2\beta + \gamma + \alpha = 2$ and $d\nu + \alpha = 2$, give very consistent values of $\alpha = -0.05(3)$. Finally, we can fit $C_{H(\max)}$ to the form $C_1 + C_2 L^{\alpha/\nu}$ in order to test this estimate of α. As shown in Fig. 15 the fit with $\alpha = -0.05$ is good, thereby providing a reasonable consistency check. The fact that both the scaling and hyperscaling relations give essentially the same estimate of α is particularly important. It is known in cases where the critical phenomena cross over from one behavior to another as the transition is approached that effective exponents determined from data not taken completely in the asymptotic reduced temperature regime can satisfy the scaling *but not the hyperscaling relations.*[28]

We have determined that this model undergoes a continuous transition at T_N which is characterized by the critical exponents given in Table II. These exponent values are close to, but still significantly different from, those calculated[15] for the 3D XY model. The exponents relevant to the 3D XY universality class are listed in Table II for easy comparison. Our estimates of the exponents of the antiferromagnetic Ising model on the STL are farther removed, but still somewhat similar to those of the 3D Ising universality class. The similarity to the exponents exhibited by the 3D XY universality class is particularly

TABLE I. The transition temperatures T_N, extracted from the different observables, are given for all the lattice sizes studied.

Lattice size	6	9	12	15	18	24	30
C_H	2.912	2.892	2.890	2.896	2.900	2.909	2.913
V_L		3.094	2.991	2.948	2.937	2.924	2.922
χ	3.160	3.047	2.994	2.967	2.963	2.951	2.946
O'	3.117	2.994	2.959	2.940	2.939	2.931	2.930
$(O^2)'$	2.999	2.918	2.905	2.906	2.906	2.907	2.912
$(\ln O)'$	3.355	3.126	3.034	2.993	2.981	2.963	2.954
$(\ln O^2)'$	3.389	3.145	3.045	3.000	2.987	2.966	2.957

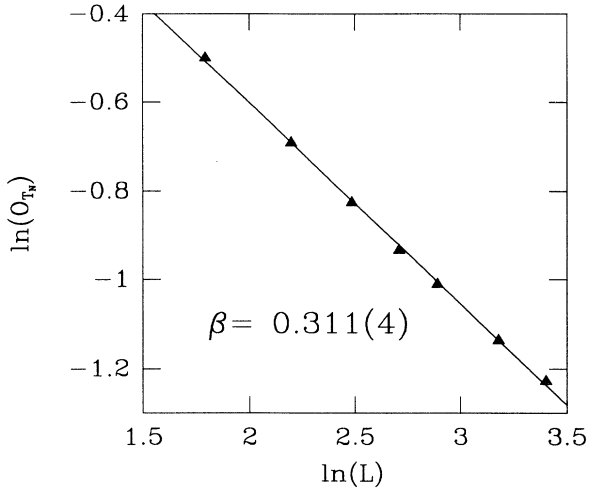

FIG. 14. The critical exponent β is determined to be 0.311(4) from the slope of the $\ln O_{T_c}$ vs $\ln L$ plot, where O_{T_c} is the order parameter evaluated at T_c=2.920.

interesting and important as previous symmetry arguments made with respect to this model indicated that the critical behavior for this model should be the 3D XY universality class.[10]

We can add confidence to our estimates for β, γ, and ν by applying the full finite scaling laws given by Eqs. (24) and (25). This is done in Figs. 16 and 17, in which $\ln(\chi L^{\gamma/\nu})$ and $\ln(OL^{\beta/\nu})$ are plotted against $\ln(tL^{1/\nu})$. The results which rely on β converge onto one line much better than those which rely on γ. This is expected since the estimate for β is more accurate than is the estimate for γ. The results are also plotted for comparison using the calculated 3D XY critical exponents,[15] in Figs.

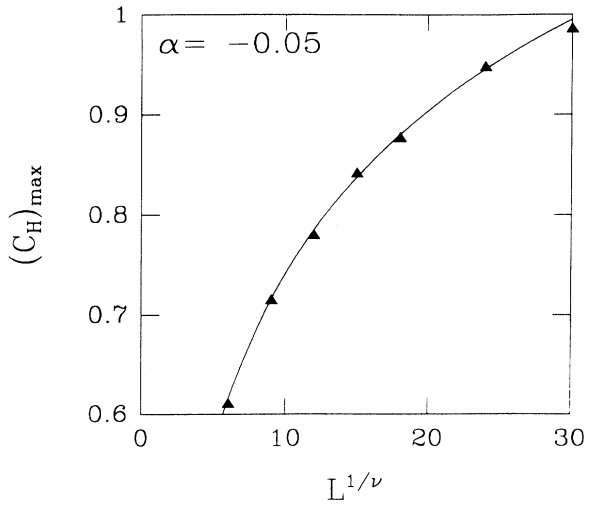

FIG. 15. The critical exponent α is determined by fitting the peak value of the specific heat $(C_H)_{\max}$ to the form $C_1 + C_2 L^{\alpha/\nu}$, where ν has already been determined to be 0.685. The solid curve shows the fit with $\alpha = -0.05$.

TABLE II. The critical exponents determined from this Monte Carlo (MC) study are given. For comparison, the exponents of the 3D XY model from Ref. 15 and the tricritical exponents from Ref. 12 are also given.

	MC	3D XY	Tricritical
α	-0.05(3)	-0.007(9)	0.5(1)
β	0.311(4)	0.346(9)	0.19(10)
γ	1.43(3)	1.316(9)	1.15(5)
ν	0.685(3)	0.669(3)	0.47

16 and 17. In this case the convergence onto a single line is easily seen to be inferior to that achieved using our carefully determined estimates for the critical exponents. Therefore to the extent that both our Monte Carlo exponent estimates as well as the theoretical values for the critical exponents of the 3D XY model are free from systematic errors, the transition at T_N in the Ising STL antiferromagnet does not belong to the 3D XY universality class. In addition, we see no evidence of tricritical mean field-like behavior, as had been reported previously.[12] The values predicted from this study[12] are also listed in Table II. If we take seriously the quoted uncertainties in the exponent estimates from both our own Monte Carlo work and the theoretical work on the 3D XY model, then the critical exponent values produced by the present work do not correspond to those of any universality class that we know of. Therefore a possible interpretation of these results is that a new universality

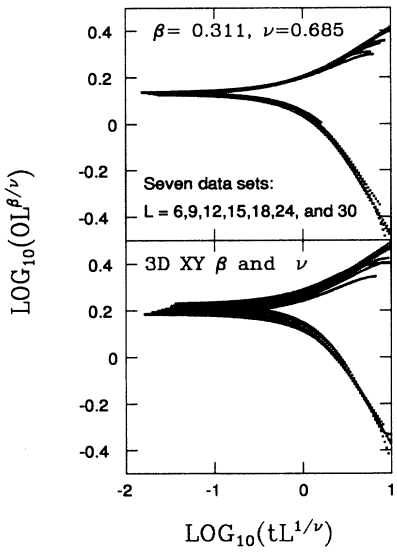

FIG. 16. The full scaling laws are checked by plotting $\ln(OL^{\beta/\nu})$ as a function of $\ln(tL^{1/\nu})$, using the exponents determined from our Monte Carlo studies, $\beta = 0.311, \nu = 0.685$. For comparison, the same plot is shown using the values theoretically estimated for the 3D XY model, $\beta = 0.346(9), \nu = 0.669(3)$. This comparison shows that the exponents determined from MC simulations provide a noticeably better fit to the scaling relations than do those calculated for the 3D XY model.

class may be relevant for this remarkably simple model of a frustrated antiferromagnet. However, we should emphasize that we cannot rule out the possibility that the discrepency between our exponents and those of the 3D XY model results from systematic errors in either our calculation, which would then have to be substantially larger than the statistical errors, or in the estimates obtained from theory.[15] This possibility can only be ruled out by further studies, with a different approach to the problem.

E. Real-space spin and soliton correlations

Considerable insight into what physical mechanism is relevant for a given phase transition can be obtained by examining the real-space spin correlations in the vicinity of the phase transition. This is particularly interesting for the model in question, as the transition we are interested in, at T_N, is one from a paramagnetic state to a long-range ordered state in which one of the three sublattices is disordered. Recent inelastic neutron-scattering measurements[29] have been made on $CsCoBr_3$, which focused on the behavior of the low-lying soliton excitations, and the role that these excitations play in mediating the phase transition seen in this material. These solitons are anti-phase-domain walls which can propagate easily along the quasi-one-dimensional antiferromagnetic chains which this material displays along its stacking direction. They are "topological" solitons, as opposed to solutions of a particular nonlinear differential equation. These measurements indicate that the development of correlations between the solitons is responsible for this transition. Specifically, they indicate that the paramagnetic state is characterized by a homogeneous and random distribution of domain walls, or solitons, along all the magnetic chains. According to the picture put forward by these measurements, the transition occurs by a bunching together, or phase separation, of the solitons along the chains, forming soliton-rich and soliton-depleted regions along all of the chains. The ordered phase forms as interchain correlations, between soliton-rich regions on one chain and appropriate soliton-depleted regions on the other two sublattice chains, develop locally.

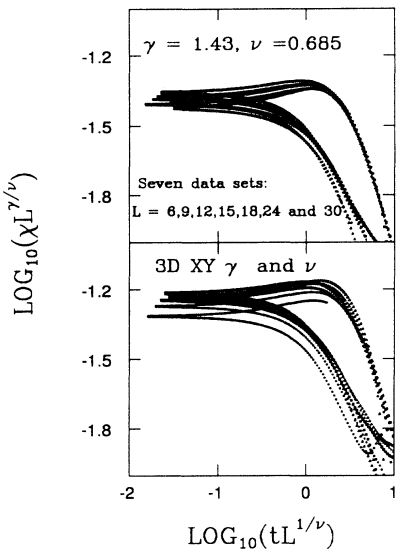

FIG. 17. The scaling laws are checked by plotting $\ln(\chi L^{\gamma/\nu})$ as a function of $\ln(tL^{1/\nu})$. In the upper part of the figure, the exponents determined from the Monte Carlo studies, $\gamma = 1.43$ and $\nu = 0.685$, are used. For comparison, the same plot is shown using the values estimated theoretically for the 3D XY model, $\gamma = 1.316$ and $\nu = 0.669$. This comparison demonstrates that the scaling laws are satisfied better with the exponents determined from MC simulations than with those calculated for the 3D XY model.

Real-space spin configurations were generated in our Monte Carlo simulation in order to look for precisely these sorts of correlations developing near the transition. As the material that was studied experimentally was quasi-one-dimensional, we chose to study this on both the isotropic model, with $J_0 = J_1 = 1.0$, as well as on a weakly one-dimensional model, $J_0 = 1.0$, $J_1 = 3.0$. Our model has ferromagnetic interactions along the stacking, or c, direction which means that a soliton, or anti-phase-domain wall, is a pair of neighboring antialigned spins along the c direction. As we are interested in the correlations between solitons we transform our spin lattice into a soliton lattice wherein we replace all nearest-neighbor pairs of antialigned spins along the c directions with a 1, indicating the presence of a soliton, and all nearest-neighbor aligned spins, representing a nonsoliton, along the c direction with 0. We then look for the emergence of structure in the soliton-soliton pair correlation function, as the transition temperature is approached.

We chose to calculate the following one-dimensional, differential soliton correlation function:

$$\Delta C_{\mathrm{sol}}(r_c) = \frac{\langle S_i S_{i+r_c}\rangle - \overline{\langle S_i S_{i+\Delta}\rangle}}{\overline{\langle S_i S_{i+\Delta}\rangle}}, \tag{28}$$

where the S_i refer to the soliton degree of freedom, either 0 or 1, described above. This quantity measures the difference between the soliton-soliton correlations over a particular distance r_c and those averaged over all distances. This is then normalized to the average soliton-soliton correlation. As such we have

$$\langle S_i S_{i+r}\rangle = \frac{1}{L}\sum_{i=1}^{L} S_i S_{i+r}, \tag{29}$$

$$\overline{\langle S_i S_{i+\Delta}\rangle} = \frac{1}{L'}\frac{1}{L}\sum_{\Delta=0}^{L'}\sum_{i=1}^{L} S_i S_{i+\Delta}. \tag{30}$$

The precise value of L' which appears in the sum over Δ is unimportant provided it is the same for all comparisons. However, it should be large compared to the largest value of r_c which we are interested in, ~ 10, and smaller than half of the chain length, $L/2 = 300$, so that the periodic boundary conditions do not unduly effect the average. For the $J_1 = 3$ lattice T_N was found to be ≈ 5.14. For both $J_1 = 1$ and $J_1 = 3$, lattices of dimensions $9 \times 9 \times 600$

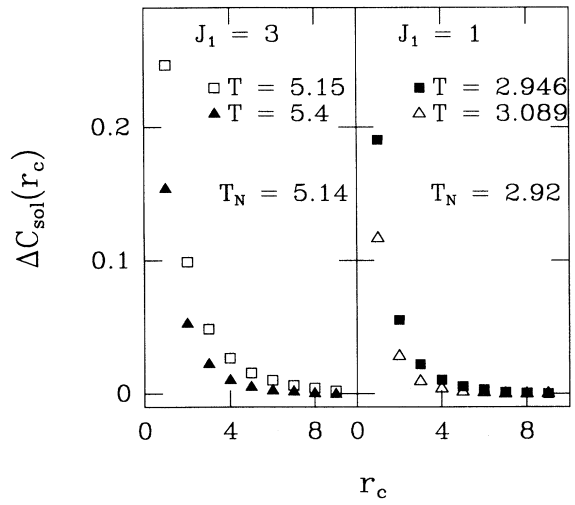

FIG. 18. The relative deviation from the average solition correlation, $\Delta C_{\rm sol}(r_c)$, is shown as a function of distance along the c axis measured in nearest-neighbor spacings. The correlation is shown for two temperatures above T_N, for the isotropic case $J_1 = 1$ and for $J_1 = 3$. The correlation is seen to increase at small r as the temperature is lowered towards T_N.

were used with 10^4 initialization steps and 3×10^3 sampled states. The one-dimensional $\Delta C_{\rm sol}(r_c)$ was calculated by averaging over the $9 \times 9 = 81$ magnetic chains that made up the three-dimensional lattice. The soliton correlation function was found at $T = 2.946$ and 3.089 for $J_1 = 1$ and at $T = 5.15$ and 5.4 for $J_1 = 3$. These results are shown in Fig 18. As the temperature approaches T_N from above, $\Delta C_{\rm sol}(r_c)$ rises at small r_c for both J_1 values. The effect is somewhat more marked in the $J_1 = 3$ case, and therefore the quasi-one-dimensionality of the system appears to accentuate the effect. Of course, the solitons themselves are thermally activated excitations so that as the temperature is lowered the soliton density, and thus the soliton-soliton correlation function averaged over all distances, must decrease. The differential correlation function takes this effect into account and shows the correlations between solitons over a particular distance, relative to the average of such correlations over all distances.

These results indicate that as the temperature decreases towards T_N the solitons coalesce and are expelled out of growing ordered regions. Thus the magnetic chains along the stacking direction do indeed separate into relatively ordered and disordered regions. We therefore conclude that the interpretation of the inelastic neutron-scattering data of the soliton response near T_N in $CsCoBr_3$ (Ref. 29) is likely correct.

IV. CONCLUSIONS

We have studied the nearest-neighbor antiferromagnetic Ising model on a STL by multiple-histogram Monte Carlo methods and finite-size scaling. Our analysis was performed on $L \times L \times L$ lattices, with $L = 6$, 9, 12, 15, 18, 24, and 30. This model was known to undergo two transitions to long-range ordered states at low temperatures. Our interest was to investigate the critical phenomena associated with the the transition from the paramagnetic to the partially paramagnetic, ordered state at T_N. We found this transition to be continuous at $T_N = 2.920(5)$ in units of $J_0 = J_1 = 1.0$, and characterized by the critical exponents $\beta = 0.311(4)$, $\gamma = 1.43(3)$, $\alpha = -0.05(3)$, and $\nu = 0.685(3)$. While these results are close to those calculated[15] for the 3D XY model, the same universality to which this model was predicted to belong, there are significant differences. As stated earlier, there are two possible reasons for this discrepancy. Systematic errors may be present in the calculation and analysis associated with producing the Monte Carlo exponent estimates, or the theoretical 3D XY estimates,[15] or both, and these may account for the differences between the theoretical 3D XY model and those calculated by this simulation work. Alternatively, this remarkably simple model of a frustrated antiferromagnet may display novel critical phenomena which is evidence for a new universality class.

It should be noted that our estimated exponents are self-consistent, in that they obey both scaling and hyperscaling relations. Also a full finite-size scaling analysis shows our data to be significantly better described by the Monte Carlo estimates than those calculated by the 3D XY model.[15] Thus we can confidently conclude that the 3D XY exponents lie outside the range of our statistical errors and also our exponent estimates do not appear to be influenced by any possible nearby multiple-critical points.[13]

Comparison to relevant experimental systems is less satisfying, mostly due to the fact that the experimental field is not itself settled. However the role of the soliton excitations on mediating the unusual transition at T_N which arose from inelastic neutron scattering measurements on $CsCoBr_3$ was seen to be qualitatively similar in the simulated model.

After this work was completed, we received a preprint (which has now affected) by Plumer *et al.*[30] in which they report on work that reproduces some of our results. Since only a single histogram at each lattice size is used in their work, their estimated exponents are expected to be less accurate than those presented in this study. However, even so, we note that their exponents are noticeably closer to the exponents we obtained from our multiple-histogram studies than to those calculated for the 3D XY model. For the case of each exponent, the deviation from those estimated for the 3D XY model is in the same direction as ours.

ACKNOWLEDGMENTS

We wish to thank D. P. Belanger and J. Wang for making available to us their heat capacity results on $CsCoBr_3$ prior to publication. We would also like to thank M. L. Plumer and collaborators for communicating the results

of their study prior to publication. In addition, we would like to thank D. P. Belanger, A. J. Berlinsky, and J. N. Reimers for many helpful comments, and J. N. Reimers for a critical reading of the manuscript. This work was supported in part by the Natural Sciences and Engineering Research Council of Canada and by the Ontario Centre for Materials Research. One of us (B.D.G.) acknowledges the support of the Alfred P. Sloan Foundation.

[1]G.H. Wannier, Phys. Rev. B **79**, 357 (1950).
[2]I. Syozi, in *Phase Transitions and Critical Phenomena*, edited by C. Domb and M.S. Green (Academic, New York, 1972), p. 269.
[3]P.W. Anderson, Phys. Rev. **102**, 1008 (1956).
[4]H. Kawamura, J. Appl. Phys. **63**, 3086 (1988); H. Kawamura, Phys. Rev. B **38**, 4916 (1989); H. Kawamura, A. Caille, and M. Plumer, *ibid.* **41**, 4416 (1990).
[5]T.E. Mason, B.D. Gaulin, and M.F. Collins, Phys. Rev. B **39**, 586 (1989); B.D. Gaulin, T.E. Mason, M.F. Collins, and J.Z. Larese, Phys. Rev. Lett. **62**, 1380 (1989); J. Wang, D.P. Belanger, and B.D. Gaulin, *ibid.* **66**, 3195 (1991).
[6]P. Azaria, P. Delamotte, and T. Jolicoeur, Phys. Rev. Lett. **64**, 3175 (1990).
[7]J.N. Reimers, J.E. Greedan, and M. Björgvinsson, Phys. Rev. B **45**, 7295 (1992).
[8]J.N. Reimers, Phys. Rev. B **45**, 7287 (1992).
[9]R. Liebmann, in *Statistical Mechanics of Periodic Frustrated Ising Systems*, edited by H. Araki, J. Ehlers, K. Hepp, R. Kippenhahn, H.A. Weidenmüller, and J. Zittartz (Springer, Berlin 1986), p. 117.
[10]A.N. Berker, G.S. Grest, C.M. Soukoulis, D. Blankschtein, and M. Ma, J. Appl. Phys. **55**, 2416 (1984); D. Blankschtein, M. Ma, A.N. Berker, G.S. Grest, and C.M. Soukoulis, Phys. Rev. B **29**, 5250 (1984).
[11]O. Nagai, J.J. Kim, K. Nishino, and Y. Yamada, J. Phys. (Paris) **49**, 1483 (1988).
[12]O. Heinonen and R.G. Petschek, Phys. Rev. B **40**, 9052 (1989).
[13]R.R. Netz and A.H. Berker, Phys. Rev. Lett. **66**, 377 (1991).
[14]S.N. Coppersmith, Phys. Rev. B **32**, 1584 (1985).
[15]G.A. Baker, Jr., B.G. Nickel, and D.I. Meiron, Phys. Rev. B **17**, 1365 (1978); see also J.C. LeGuillou and J. Zinn-Justin, Phys. Rev. Lett. **39**, 95 (1977).
[16]S.E. Nagler, W.J.L. Buyers, R.L. Armstrong, and B. Briat, Phys. Rev. B **27**, 1784 (1983).
[17]M. Mekata and K. Adachi, J. Phys. Soc. Jpn. **44**, 806 (1978).
[18]W.B. Yelon, D.E. Cox, and M. Eibshutz, Phys. Rev. B **12**, 5007 (1975).
[19]A. Farkas, B.D. Gaulin, Z. Tun, and B. Briat, J. Appl. Phys. **69**, 6167 (1991).
[20]J. Wang, D.P. Belanger, and B.D. Gaulin (unpublished).
[21]G. Ahlers, Rev. Mod. Phys. **52**, 489 (1980).
[22]A.M. Ferrenberg and R.H. Swendsen, Phys. Rev. Lett. **61**, 2635 (1988).
[23]A.M. Ferrenberg and R.H. Swendsen, Phys. Rev. Lett. **63**, 1195 (1989).
[24]J. Lee and J.M. Kosterlitz, Phys. Rev. Lett. **65**, 137 (1990); Phys. Rev. B **43**, 3265 (1991).
[25]M. Fukugita, H. Mino, M. Okawa, and K.A. Ukawa, J. Phys. A. **23**, L561 (1990).
[26]M.E. Fisher, in *Critical Phenomena*, edited by M.S. Green (Academic, New York, 1971); M.E. Fisher and M.N. Barber, Phys. Rev. Lett. **28**, 1516 (1972).
[27]D.P. Landau, Phys. Rev. B **13**, 2997 (1976); **14**, 225 (1976).
[28]A. Aharony and G. Ahlers, Phys. Rev. Lett. **44**, 782 (1980).
[29]Z. Tun, B.D. Gaulin, R.B. Rogge, and B. Briat, J. Magn. Magn. Mater. **104-107**, 1045 (1992).
[30]M.L. Plumer, A. Mailhot, R. Ducharme, A. Caille, and H.T. Diep, Phys. Rev. B **47**, 14312 (1993).